Published in IET Microwaves, Antennas & Propagation
Received on 4th March 2013
Revised on 25th November 2013
Accepted on 26th November 2013
doi: 10.1049/iet-map.2013.0104

ISSN 1751-8725

Shaped beam array synthesis using particle swarm optimisation method with mutual coupling compensation and wideband feeding network

Abbas Pirhadi[1], *Mohammad Hassan Rahmani*[1], *Alireza Mallahzadeh*[2]

[1]*Faculty of Electrical and Computer Engineering, Shahid Beheshti University G.C (SBU), Tehran, Iran*
[2]*Faculty of Engineering, Shahed University, Tehran, Iran*
E-mail: a_prhadi@sbu.ac.ir

Abstract: This work presents the design, simulation and implementation of a linear array antenna with a fully constrained cosecant squared radiation pattern and a novel wideband feeding network. This antenna is constructed of wideband printed dipole antennas as the array elements in which the mutual coupling effect is properly compensated. For this purpose, a constrained particle swarm optimisation (PSO) algorithm is used as the synthesis method which is able to deal with multiple constraints in the desired radiation pattern. The excitations obtained from the PSO algorithm are applied to the design of a wideband feeding network which is able to deliver stable phase shifts and output powers to the array elements over the desired bandwidth. Finally, the simulation results are confirmed by the measurement results.

1 Introduction

Now a days, shaped beam radiation pattern is an important research topic in wireless communication. This has made a tendency towards using array antennas, because of their versatility, ease of implementation and low cost [1]. The design approach to obtain a specific radiation pattern for the array antennas is finding the elements excitations (i.e. elements phase and amplitude), as well as the position of elements [1]. To date, several analytical and numerical methods have been proposed to address this issue [1, 2]. However, in recent years most of the researches have been devoted to the application of evolutionary optimisation methods such as genetic algorithm, differential evolution and particle swarm optimisation (PSO) in the field of array antenna synthesis [3–6].

The design and synthesis of an array antenna for a desired radiation pattern are affected by the mutual coupling between the elements which results in a difference between the theoretical synthesis and the practical implementation [7]. Considering the mutual coupling effect is not a computationally straightforward task and could be prohibitively time consuming. The coupling effect is mainly determined by the number of array elements and their geometry. It is worth noting that the coupling effect is more important in small array antennas with fewer elements and can result in unwanted effects including beam widening, gain decrease and side lobe level increase [8–10].

The PSO algorithm is attractive because of its fast and precise convergence, simple calculation steps and easy implementation which are the result of the Newtonian law of motion in this algorithm [11, 12]. This method has been used in different electromagnetics applications in the last decade, including array antenna synthesis. In contrast with other stochastic algorithms, the PSO is proved to be easier to understand, adjust and implement. Moreover, with a good choice of initial values, the PSO can be guided to a desired result with a better time efficiency [11–15]. In this work, the PSO is used in order to synthesise the array antenna to obtain the shaped radiation pattern.

Design of the feeding network is a critical part of the array antenna design because the bandwidth of the whole system is highly dependent on it. Various methods have been used to design and implement the feeding network. However, for a shaped beam radiation pattern the feeding network design would be more difficult. Digital phase shifters and attenuators are not always able to deliver the exact amounts of powers and phase shifts that are defined by the optimisation method in the whole frequency band [16]. The usage of Wilkinson power dividers and delay line phase shifters has the advantage of delivering the exact power. However, these configurations suffer from isolation, impedance mismatch and phase variation issues over a wide frequency range [17]. In this paper, a feeding network with Wilkinson power dividers and special delay line phase shifters is proposed to operate in a wide frequency band.

The organisation of the paper is as follows. In Section 2, the application of the PSO to synthesise array antennas is discussed. In Section 3, the array antenna and its elements are presented in detail. Section 4 presents the simulation results and discusses the mutual coupling compensation by using complex active element patterns and PSO. In Section 5, the design of the wideband feeding network is

presented. Finally, in Section 6, the measurement results of the fabricated model are illustrated.

2 Using PSO to synthesise array antenna

2.1 Defining the problem

The far-field array factor for a linear array of isotropic elements positioned along the z-axis with the wave number $k = 2\pi d/\lambda$ is of the following form $\mathrm{AF}(\theta) = \sum_{n=1}^{N} A_n e^{jkn\cos\theta + j\varphi_n}$, where d is the inter-element distance, λ is the wavelength in free space, n is the element number and N is the total number of elements. A_n is the current amplitude of the nth element and φ_n is the phase of the nth element which are used to shape the radiation pattern of the array antenna. However, to consider the effect of mutual coupling in the array formulation, we need to formulate the problem in a more general form. Owing to this fact, we have to consider the amplitude and phase of the pattern of each element in the presence of other elements which is called the active pattern of the element namely $E_n(\theta, \varphi)$. In our simulations θ changes from 0° to 90° while φ is fixed at either 0° or 180°. $E_n(\theta, \varphi)$ is an embedded complex number for the nth element and must be multiplied by the amplitude and phase vector $A_n e^{j\varphi_n}$ [7, 8]

$$F(\theta, \varphi) = \sum_{n=1}^{N} A_n e^{j\varphi_n} E_n(\theta, \varphi) \tag{1}$$

Evolutionary algorithms, because of the non-linear nature of the problems, are widely used in electromagnetic. Moreover, PSO is used to optimise continuous and discrete functions. Different applications like pattern synthesis of array antenna, reflector antenna optimisation, corrugated horn optimisation, patch antenna design, frequency selective surface design and microwave absorber design are examples in the field of electromagnetics in which the PSO has been used recently [18–23].

2.2 Development of the PSO for the current work

In the conventional PSO, particles are generated randomly within the desired boundaries and they can displace freely in the solution space [11]. Although this reduces the probability of immature convergence and increases the preciseness of the method, it usually leads to non-realistic amplitudes and phases that make their implementation sometimes impossible in the synthesis of array antenna. If the relative amplitude of two adjacent elements is too high, the fabrication of the related power splitter will be difficult and practically impossible. Moreover, in the point of view of phases, large inter-element phase difference will also make the design of the wideband feeding network more difficult because it requires wideband phase shifters with large phase difference between elements.

The development of the original PSO algorithm aims to control large changes of inter-element amplitudes and phases of the excitations. In the first step of the algorithm, random phases and amplitudes as the input variable of the PSO algorithm are generated for being used in the algorithm. In the original PSO, input matrix variable ($\boldsymbol{X}_1$) is generated randomly within the imposed limitations but in our modified algorithm, to control the relative amplitude and phase difference between the elements, the domain of random selection for each element of the matrix is divided between the elements. This means that $\boldsymbol{X}_1$ is no longer a matrix of a completely random numbers between $X_{\max}$ and $X_{\min}$, but it is guided in such a way that each number is allowed to be chosen randomly in its own domain which is defined as follows

$$s = \frac{X_{\max} - X_{\min}}{n} \tag{2}$$

$$a(\mu_n) = X_{\min} + (\mu_n - 1)s \tag{3}$$

$$X = \{a(\mu_n) + (a(\mu_n + 1) - a(\mu_n))\gamma\} \tag{4}$$

In the above formulation, $\mu_n = \{1,2, ..., N\}$ according to the nth element of the array, and γ is a random number between (0, 1). $X_{\max}$ and $X_{\min}$ are, respectively, the maximum and the minimum of acceptable values for amplitudes and phases. Then, the position of the particles through the algorithm is updated using (6) and (7)

$$V_{k+1}^i = w_k V_k^i + \boldsymbol{r}_1 c_1 (\mathrm{Pb}^i - X_k) + \boldsymbol{r}_2 c_2 (\mathrm{Gb} - X_k) \tag{5}$$

$$X_{k+1}^i = X_k^i + V_{k+1}^i \tag{6}$$

where V_k^i is the velocity of the ith particle in the kth iteration, X_k^i is the position of the ith particle in the kth iteration. w_k is the weighting coefficient of the kth iteration, $\boldsymbol{r}_1$ and $\boldsymbol{r}_2$ are random matrices, and $c_1 = c_2 = 2$ are called the acceleration coefficients. Pb^i is the best position of the particle ith during its exploration and Gb is the global best of the whole group. The weighting coefficient, w, is set to change linearly based on (8)

$$w_k = w_{\max} - \frac{(w_{\max} - w_{\min})^*(k-1)}{k_{\max}} \tag{7}$$

where k is the iteration number with the maximum of $k_{\max} = 150$ while $w_{\min} = 0.2$ is the minimum value of the weighting factor, and $w_{\max} = 0.9$ is its maximum value.

As shown in Fig. 1 in order to increase the efficiency of the algorithm the desired pattern is divided into 4 regions with different weights. Multiple constraints have been imposed to this desired pattern such as different side lobe regions with the weight of $w1$, fixed slope in the broadside direction with the weight of $w2$ and specific values for the slope of coverage region with the weights of $w3$ and $w4$. The application of this radiation pattern is in air navigation radars [1].

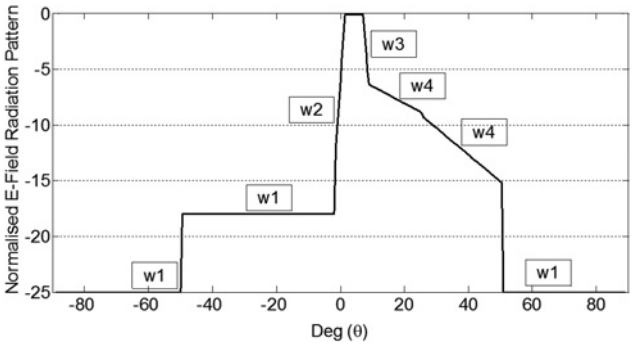

Fig. 1 *Desired pattern with different weighting parts*

doi: 10.1049/iet-map.2013.0104

The error function is calculated as

$$\text{Error} = w1\sum_{-90}^{a1}|F_d - F_N| + w2\sum_{a1+1}^{a-1}|F_d - F_N| + w3\sum_{a}^{b}|F_d - F_N| + w4\sum_{b+1}^{b1}|F_d - F_N| + w4\sum_{b1+1}^{90}|F_d - F_N| \quad (8)$$

F_d is the desired radiation pattern and F_N is the normalised calculated complex array factor which is given in each iteration using the amplitudes and phases delivered by the algorithm. $w1$, $w2$, $w3$ and $w4$ are the weights given to each part depending on the necessary resolution.

3 Antenna and array configuration

The designed array consists of 11 elements of wideband printed dipole antenna (PDA) with balun working at the centre frequency of 1.1 GHz. It has been generally proved that a dipole antenna needs a balanced feed that could be a $\lambda/4$ coaxial balun [1]. For a printed dipole this could be replaced by an integrated balun with a broadband performance which has been used in different antenna array applications [24, 25]. To achieve a better impedance matching with wideband performance, instead of using quarter wavelength transformers, the feed point of the integrated balun is adjusted as described in [26]. The PDA element, the array configuration and the |S_11| plot of the single PDA are shown in Fig. 2. Changing the parameters H4 and H3 will lead to a wideband |S_11|.

In the array configuration, the inter-element distance (d) is 0.8λ for a centre frequency of 1.1 GHz. The antenna is printed on a Ro4003 substrate with $\varepsilon_r = 3.38$ and a thickness of .82 mil. Moreover, a ground plane is used in the array structure in order to increase the array directivity. The simulation and analysis have been performed by the EM software HFSS based on the finite element method.

4 Simulation procedure

4.1 Array synthesis with an investigation of the mutual coupling effect

In practice, mutual coupling causes the difference between the radiation patterns of elements in the array. To compensate this effect, we have used complex active element patterns. The active pattern of each element is derived in the array, using the HFSS, by exciting it in the presence of other elements. Inserting the active patterns in (2), causes the mutual coupling to be considered during the optimisation. As an example, the active radiation patterns of elements 1, 3 and 5, for both amplitude and phase are shown in Figs. 3*a* and *b*, respectively. As the symmetric geometry of the array, the elements on the one half of the array will have the same mirrored patterns with respect to the *XZ*-plane. It is observed that the far-field pattern of each element is different from the others.

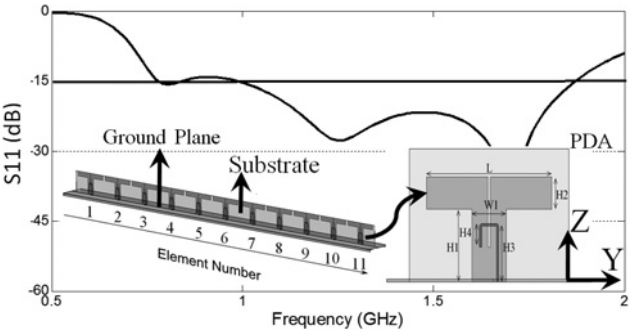

Fig. 2 *Single microstrip dipole (on the right) and its |S_11| Plot. (with H1 = 52 mm, H2 = 23 mm, H3 = 40 mm, H4 = 15.3 mm, W1 = 30 mm and L1 = 110 mm) and 11 elements array configuration (on the left) with ground plane dimensions = 1706 mm*110 mm*

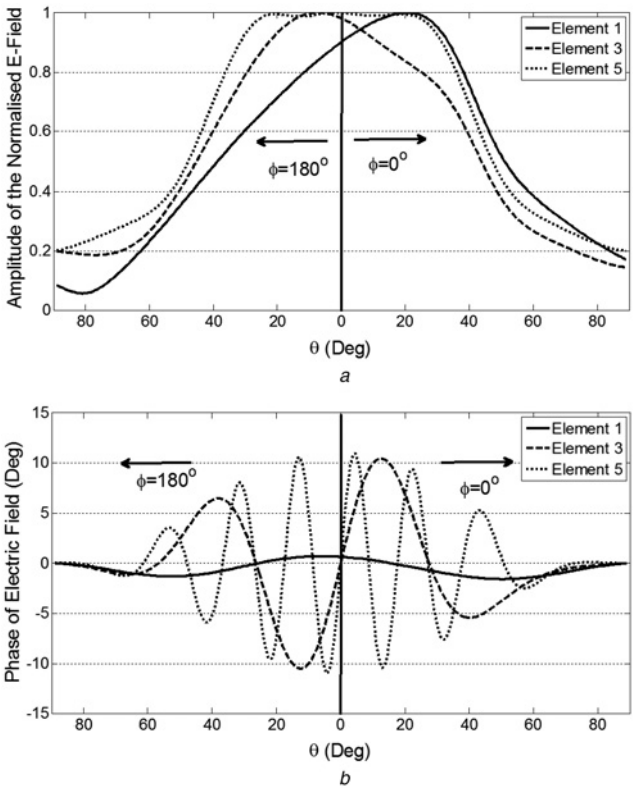

Fig. 3 *Radiation pattern of printed dipoles*

a Normalised *E*-fields of elements 1, 3 and 5 in the array
b Phase of *E*-field of elements 1, 3 and 5 in the array

4.2 Simulation and optimisation results

The result of the optimisation procedure is depicted in Fig. 4.

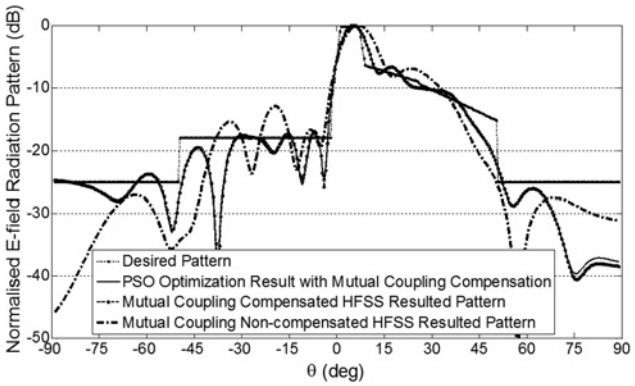

Fig. 4 *Radiation pattern of normalised E-field of 11 elements MDA with far field mutual coupling consideration*

Table 1 Excitation amplitudes and phases of the array before and after mutual coupling compensation

Element number	Normalised amplitude		Phase, deg.	
	Before mut. coupl. compensation	After mut. coupl. compensation	Before mut. coupl. compensation	After mut. coupl. compensation
1	0.72	0.3	275.2	274.5
2	0.94	0.24	280.1	211.2
3	1	0.35	275.1	246.5
4	0.76	1	250.3	186.9
5	0.52	1	248.2	132.7
6	0.63	0.33	222.8	87.25
7	0.63	0.12	221.2	102.2
8	0.4	0.16	219.7	120.9
9	0.38	0.16	154.3	118.9
10	0.38	0.16	110.6	53.33
11	0.27	0.16	59.3	59.44

Fig. 4 shows that taking into account the mutual coupling effect in the PSO process leads to a good agreement between the optimisation and HFSS results while not taking it into account will result in a degraded final radiation pattern. The optimisation was performed with 150 iterations and converged in less than 50 iterations which shows the high speed of this algorithm. The derived amplitudes and phases before and after considering the mutual coupling effect are shown in Table 1. It is seen that, by using the suggested method for deriving the initial values of the PSO, the level of changes in the amplitude is controlled between 0.3 and 1. Moreover, phases change linearly between 53.33° and 274.5°. This eases the design of the feeding network, as is described in the next section and increases the accuracy of the calculated radiation pattern.

5 Design of the feeding structure

Having obtained the optimum amplitudes and phases of the array elements, it is necessary to design a suitable feeding network. In this case, as a result of using the PSO with the described modifications in the initial values, large changes in the relative amplitudes of elements and phase differences between the elements are avoided. The inter-element phase shift is approximately linear and limited so the phase shifters are easier to design. Moreover, the relative amplitudes are limited so that the design and implementation of power dividers are possible using common printed transmission line such as the microstrip lines. In the following section, the feeding network, the power dividers and the phase shifters have been simulated and analysed by the HFSS EM software.

The feeding network consists of several power dividers. The optimum tapering of amplitude of the array elements is obtained by adjusting the ratio of power division in the power dividers. As mentioned earlier, the mutual coupling effects of the embedded array elements are compensated during the PSO optimisation procedure by considering the active radiation pattern. However, the inter-port coupling is an important issue that greatly affects the performance of the designed array. To minimise this effect, the Wilkinson power dividers are used in the proposed structure which provides two isolated ports with minimum inter-port coupling [27].

In addition, to obtain the optimum phase distribution, it is necessary to adjust the length of each path of the feeding network. The most challenging part in the design of the feeding network is its phase stability in the whole frequency bandwidth. For this application, the desired bandwidth is about 30% with the centre frequency of 1.1 GHz. To achieve this performance, it is required to design

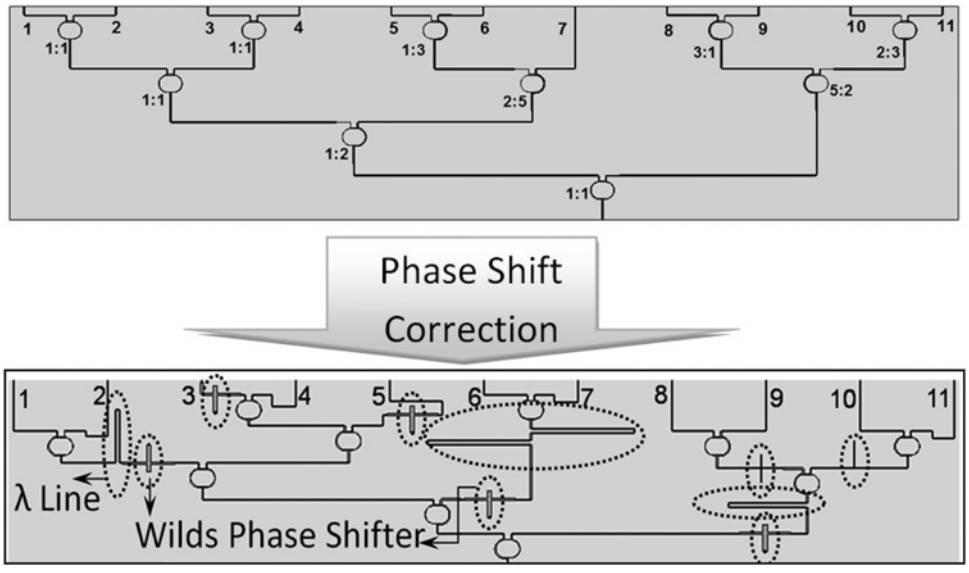

Fig. 5 *Schematic view of the feeding network before and after phase shifts corrections*

doi: 10.1049/iet-map.2013.0104

wideband phase shifters and use them to fix the desired phase shift. The designed feeding networks at the centre frequency before and after adding the wideband phase shifters are shown in Fig. 5. Design of feeding network includes two steps. In the first step, the optimum amplitudes in the second column of Table 1 are implemented and in the second step, the designed feeding network is modified to obtain the optimum phase in the fourth column of Table 1. The details of feeding network design are represented in the next section.

5.1 Designing the feed network at the centre frequency

To design the feeding network at the centre frequency (Fig. 5-top), equal and non-equal Wilkinson power dividers are separately designed and analysed with the desired power splitting ratio and phase shift at the centre frequency. The desired power splitting ratios are obtained by using the formulation in [28], and the desired phase shifts are obtained through adjusting the length of the microstrip lines at the centre frequency. For obtaining the power dividing ratios, we used the normalised amplitudes after mutual coupling compensation in Table 1. By separating the nearby elements two by two and dividing their amplitudes the splitting ratios of the power dividers are obtained and this procedure continues for the next levels. Then, the whole feed network is made by uniting these separate power dividers. In this step, the feeding network delivers the proper power to each element with the desired phase shift at the centre frequency. The output powers of this feeding network over the desired frequency band are shown in Fig. 6.

The results show that the output power produced at each port is nearly stable over the whole frequency band and does not need correction. Moreover, it can be verified that the resulted powers comply with the reference desired powers in Table 1. Fig. 7 shows the resulted phase shift for each port.

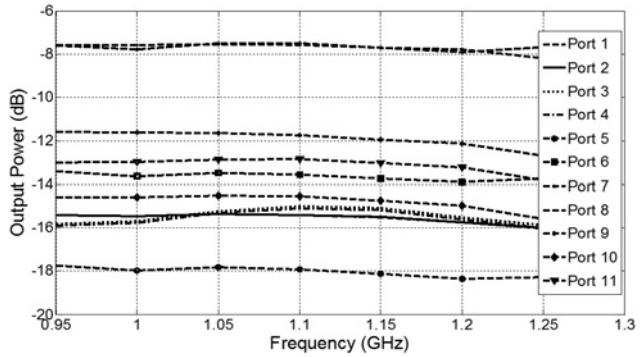

Fig. 6 *Resulted output power at each port*

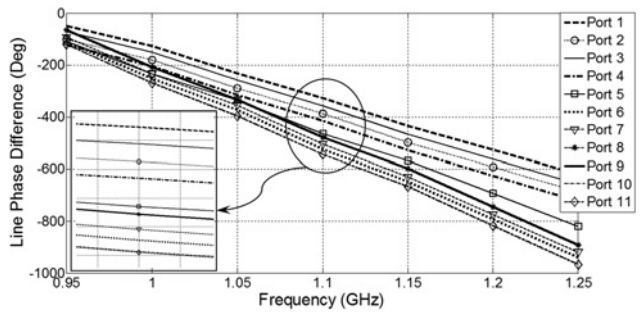

Fig. 7 *Resulted output phase shift of each port*

As shown in Fig. 7, because of the different path lengths, the phase difference between the ports are not stable over the whole frequency band and the phase variation slopes are not the same for all ports. This degrades the resulted radiation pattern in the frequency band and thus the phase shift correction is required.

5.2 Output phase difference correction within the desired bandwidth

Correcting the resulted phase differences in such a way that they become stable over the whole frequency band involves different stages. First, we have to find the reference port which is the one with the maximum slope. Here, the reference port is port no.4 as it has the longest length. Then, by increasing the length of the microstrip lines in other routes and also using wideband phase shifters, we have to increase the phase slope of other ports to acquire the reference slope. It is worth noting that this correction procedure must be done in such a way that the phase differences do not change at the centre frequency.

According to (9), the produced phase shift of a microstrip line is a linear function of frequency. This is used in the above procedure to increase the slope of the output phase when needed

$$\beta l = \frac{2\pi}{\lambda_g} = \frac{2\sqrt{\varepsilon_e}\pi}{\lambda} = \frac{2\sqrt{\varepsilon_e}\pi}{C} l \times f \tag{9}$$

where β is the propagation constant, λ_g is the guided wavelength of the microstrip line, λ is the free space wavelength, ε_e is the effective dielectric constant, C is the free space wave velocity and f is the frequency. However, to avoid phase shift variation at the centre frequency, we can only use lines with $L = n\lambda$ that produce a $2n\pi$ phase shift. These lines can add phase differences between the beginning and the end of the bandwidth for 100° and are used for paths which need more than 100° phase shift slope corrections compared with the reference paths.

The wideband phase shifter consists of a Wilds phase shifter which is fully described in [29]. It consists of two $\lambda/8$ stubs (one short circuited to the ground layer and the other left open) or one open ended $\lambda/4$ stub. When we add this element in the transmission line path, by changing L_1/L_2 in Fig. 8, we can increase the slope of the phase shift of the simple TL. Fig. 8 shows the typical phase shift slope correction by these phase shifters in which the two-stubs and one-stub configurations increase the phase shift in the whole frequency band about 25° and 12°, respectively, with respect to the simple TL.

5.3 Design of wideband feeding network

As shown in Fig. 7, prior to slope correction, the slope of the phase shift for each port over the frequency band is different. By correcting the phase shift as described in the preceding section, a wideband feeding network with stable phase shift and power split ratio is obtained.

The reference port for the phase shift correction is port no.4 as it has the longest path from the input port. In order to reach this reference, first, a microstrip line with $L_1 = \lambda$ has been added in the paths of ports 8, 9, 10 and 11 to increase the slope of the output phase shift for these ports. By

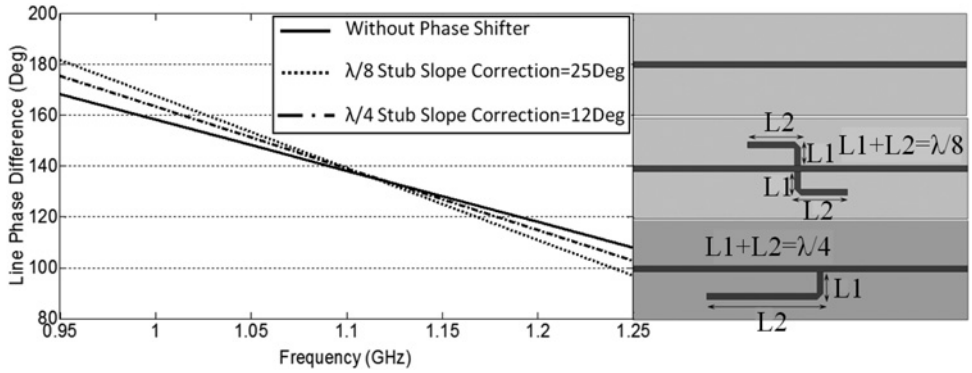

Fig. 8 *Wilds phase shifters and their phase difference corrections*

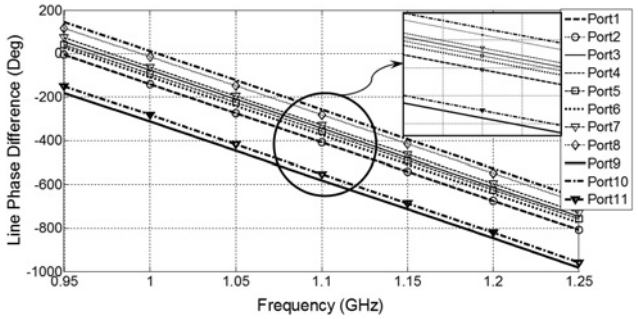

Fig. 9 *Output phase shift of each port after correction*

comparing the port no.4 and ports nos. 6 and 7, it is understood that an addition of microstrip line with $L_2 = 2\lambda$ is needed in this path. Another line with $L_3 = \lambda$ is needed in the path of ports 1 and 2. The next step is to start from the top to the bottom and compare the phase shift slope of each arm of the power divider and use a proper Wilds phase shifter to fine tune the phase shift differences over the frequency band. Fig 9 shows the final result for the output phase shifts in the whole frequency band.

As it is demonstrated in Fig. 9, when the phase shift is corrected, the slopes of the output phase shifts for all ports are finally identical, and consequently, the phase differences between ports are stable within the whole frequency band.

Table 2 Optimised values and feeding network resulted normalised amplitudes and phases of excitations

Element number	Normalised amplitude		Phase, deg.	
	Feeding net.	Optimised values	Feeding net.	Optimised values
1	0.28	0.3	267.2	274.5
2	0.20	0.24	203.9	211.2
3	0.37	0.34	247	246.5
4	1	1	187	186.9
5	0.99	0.99	130.5	132.7
6	0.25	0.32	86.72	87.25
7	0.09	0.12	102	102.2
8	0.18	0.16	122.7	120.9
9	0.18	0.16	122.5	118.9
10	0.17	0.16	58.97	53.33
11	0.17	0.16	59	59.44

The final results are shown in Table 2. It is seen that the resulted phase and amplitudes comply with the desired optimisation values.

6 Fabrication and measurement results

According to the design procedure described in the previous section, the PDA array together with its feeding network has been fabricated and analysed. Fig 10 shows the final fabricated array antenna structure.

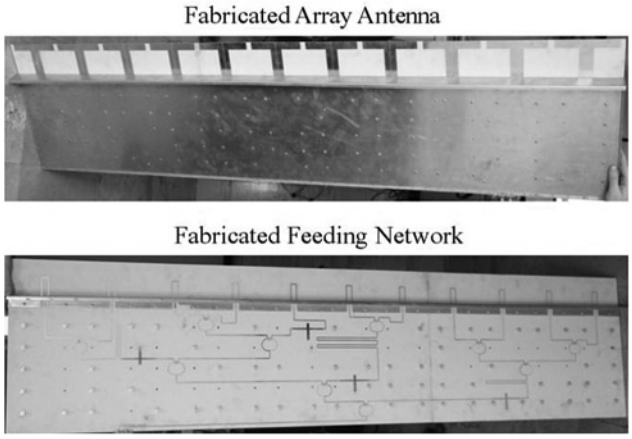

Fig. 10 *Front view and back view of the fabricated array antenna and feeding network*

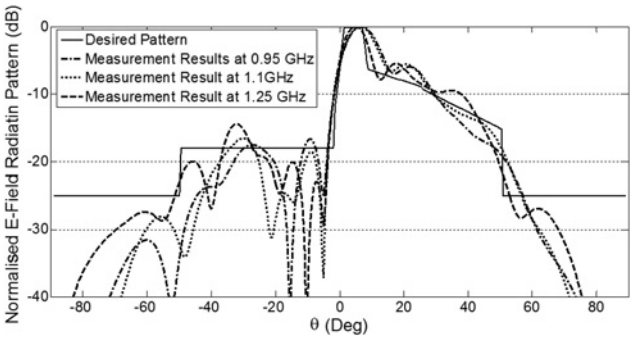

Fig. 11 *Measured normalised electric field radiation pattern at $f = 0.95$ GHz, $f = 1.1$ GHz and 1.25 GHz*

doi: 10.1049/iet-map.2013.0104

The final measurement of normalised *E*-field radiation patterns are shown in Fig. 11. In this figure, the measurement results are compared for three different operating frequencies of 0.95, 1.1 and 1.25 GHz.

7 Conclusion

An accurate approach for the synthesis of shaped beam array has been proposed by taking into account the mutual coupling effect between array elements. To this aim, a combination of PSO algorithm and complex active element radiation patterns in the array was introduced to obtain a cosecant squared radiation pattern. A new method for the design of a wideband and isolated feeding network has been proposed and implemented with equal and non-equal Wilkinson power splitters and wideband phase shifters. It has been shown that the proposed approach is robust, fast and applicable to small and medium sized arrays. It was also shown that the proposed method could be properly applied to different array structures that may cause a variation in the single element pattern through mutual coupling, the presence of external objects, radomes or other considerations. The designed array consists of 11 printed dipole antennas that operate at the central frequency of 1.1 GHz. It has been shown that the designed feeding network is able to produce a consistent cosecant squared pattern over the frequency bandwidth of 30% with the centre frequency of 1.1 GHz.

8 Acknowledgment

The authors thank the Antenna Lab of the MUT University for the support of the measurements of this work.

9 References

1 Josefsson, L., Persson, P.: 'Conformal array antenna theory and design' (IEEE Press, 2006, 1st edn.), pp. 365–389
2 Balanis, C.A.: 'Antenna theory: analysis and design' (John Wiley & Sons, 2005, 3rd edn.)
3 Ares, F.M., Rodriguez, J.A., Villanueva, E., *et al.*: 'Genetic algorithms in the design and optimization of antenna array pattern', *IEEE Trans. Antennas Propag.*, 1999, **47**, (3), pp. 506–510
4 Kurup, D., Himdi, M., Rydberg, A.: 'Synthesis of uniform amplitude unequally spaced antenna arrays using the differential algorithm', *IEEE Trans. Antennas Propag.*, 2003, **51**, (9), pp. 2210–2217
5 Gies, D., Rahmat-Samii, Y.: 'Particle swarm optimization for reconfigurable phase differentiated array design', *Microw. Opt. Technol. Lett.*, 2003, **38**, (3), pp. 168–175
6 Boeringer, D.W., Werner, D.H.: 'Particle swarm optimization versus genetic algorithms for phased array synthesis', *IEEE Trans. Antennas Propag.*, 2004, **52**, (3), pp. 771–779
7 Gupta, I.J., Ksienski, A.A.: 'Effect of mutual coupling on the performance of adaptive arrays', *IEEE Trans. Antennas Propag.*, 1983, **31**, (5), pp. 785–791
8 Kelley, D.F., Stutzman, W.L.: 'Array antenna pattern modelling method that includes mutual coupling effects', *IEEE Trans. Antennas Propag.*, 1993, **41**, (12), pp. 1625–1632
9 Darwood, P., Fletcher, P.N., Hilton, G.S.: 'Mutual coupling compensation in small planar array antennas', *IEE Proc. Microw. Antennas Propag.*, 1998, **145**, (1), pp. 1–6
10 Fletcher, P.N., Dean, M.: 'Derivation of orthogonal beams and their application to beamforming in small phased arrays', *IEE Proc. Microw. Antennas Propag.*, 1996, **143**, (4), pp. 304–308
11 Kennedy, J., Eberhart, R.: 'Particle swarm optimization'. Proc. IEEE Int. Conf. Neural Networks, Perth, Australia, 1995, pp. 1942–1948
12 Eberhart, R., Shi, Y.: 'Particle swarm optimization: developments, applications, and resources', *Proc. Cong. Evol. Comput.*, 2001, **1**, pp. 81–86
13 Perez, J.R., Basterrechea, J.: 'Hybrid particle swarm-based algorithms and their application to linear array synthesis', *Prog. Electromagn. Res.*, 2009, **90**, pp. 63–74
14 Zaharis, Z.D., Goudos, S.K., Yioultsis, T.V.: 'Application of boolean PSO with adaptive velocity mutation to the design of optimal linear antenna arrays excited by uniform amplitude current distribution', *J. Electromagn. Waves Appl.*, 2011, **25**, (10), pp. 1422–1436
15 Goudos, S.K., Zaharis, Z.D., Kampitaki, D.G., *et al.*: 'Pareto optimal design of dual-band base station antenna arrays using multi-objective particle swarm optimization with fitness sharing', *IEEE Trans. Magn.*, 2009, **45**, (3), pp. 1522–1525
16 Ismail, T.H., Hamici, Z.M.: 'Array pattern synthesis using digital phase control by quantized particle swarm optimization', *IEEE Trans. Antennas Propag.*, 2010, **58**, (6), pp. 2142–2145
17 Pozar, D.M.: 'Microwave engineering' (John Wiley & Sons, Inc., 2005, 4th edn., 2011), pp. 318–324
18 Robinson, J., Rahmat-Samii, Y.: 'Particle swarm optimization in electromagnetics', *IEEE Trans. Antennas Propag.*, 2004, **52**, (2), pp. 397–407
19 Gies, D., Rahmat-Samii, Y.: 'Particle swarm optimization (PSO) for reflector antenna shaping'. IEEE Antennas Propagation Soc. Int. Symp., California, USA, 2004, pp. 2289–2293
20 Liu, W.: 'Design of multiband CPW-fed monopole antenna using a particle swarm optimization approach', *IEEE Trans. Antennas Propag.*, 2005, **53**, (10), pp. 3273–3279
21 Genovesi, S., Mittra, R., Monorchio, A., *et al.*: 'Particle swarm optimization for the design of frequency selective surfaces', *IEEE Antennas Wirel. Propag. Lett.*, 2006, **1**, (5), pp. 277–279
22 Li, W.T., Shi, X.W.: 'An improved particle swarm optimization algorithm for pattern synthesis of phased arrays', *Prog. Electromagn. Res., PIER*, 2008, **82**, pp. 319–332
23 Sotirios, K.G., Vasiliki, M., Theodoros, S., *et al.*: 'Application of a comprehensive learning particle swarm optimizer to unequally spaced linear array synthesis with sidelobe level suppression and null control', *IEEE Antennas Wirel. Propag. Lett.*, 2010, **9**, pp. 125–129
24 Edward, B., Rees, D.: 'A broadband printed dipole with integrated balun', *Microw. J.*, 1987, **30**, pp. 339–344
25 Bayard, J.P.R.: 'Analysis of infinite arrays of microstrip-fed dipoles printed on protruding dielectric substrates and covered with a dielectric radome', *IEEE Trans. Antennas Propag.*, 1994, **42**, (1), pp. 82–89
26 Lin, L.R., Wu, T., Pan, B., *et al.*: 'Equivalent circuit analysis of a broadband printed dipole with adjusted integrated balun and an array for base station applications', *IEEE Trans. Antennas Propag.*, 2009, **57**, (7), pp. 2180–2184
27 Wilkinson, E.J.: 'An N-way hybrid power divider', *IRE Trans. MTT*, 1960, **8**, pp. 116–118
28 Parad, L.I., Moynihan, R.L.: 'Split tee power divider', *IEEE Trans. MTT*, 1965, **13**, (1), pp. 91–95
29 Wilds, R.B.: 'Try λ/8 stubs for fast fixed phase shifts', *Microw. RF*, 1979, **18**, pp. 67–68